WELDING RESEARCH

SUPPLEMENT TO THE *WELDING JOURNAL*, JANUARY 1995
Sponsored by the American Welding Society and the Welding Research Council

Effect of Postweld Heat Treatment on Ti-14%Al-21%Nb Fusion Zone Structure and Hardness

Postweld heat treatment at 650°C was found to be less effective at reducing hardness to acceptable levels than a PWHT at 980°C

BY V. L. ACOFF, R. G. THOMPSON, R. D. GRIFFIN AND B. RADHAKRISHNAN

ABSTRACT. Gas tungsten arc (GTA) spot welds were made on 1 x 0.5 x 0. 018-in. (2.54 x 1.57 x 0.0457-cm) samples of Ti-14.2Al-21.3Nb (wt-%). The samples were welded for 3 s at 32 A and 17 V. The as-welded fusion zone consisted of a ω-type, "tweed-like" microstructure with a microhardness that was higher than the base metal by as much as 100 VHN. Two postweld heat treatment (PWHT) temperatures were chosen, which represented the upper (980°C) and lower (650°C) limits of the $\alpha_2 + \beta$ region of the Ti_3Al-Nb pseudo-binary phase diagram. Short PWHT times at 650°C resulted in secondary hardening above that of the as-welded condition while longer times resulted in hardness values near that of the base metal. Only heavily faulted α_2 was detected in the 650°C PWHTs. The PWHT at 980°C produced rapid softening of the weld metal. A 1-min PWHT at 980°C had a microhardness and microstructure similar to the 650°C, 50 h PWHT. All other PWHTs at 980°C had microhardness values near that of the base metal. There were two distinct microstructures for the 980°C PWHT. One consisted of α_2 subgrains with a high dislocation density and B2 precipitates. The other consisted of clear α_2 grains with B2 at grain boundaries.

V. L. ACOFF, R. G. THOMPSON, R. D. GRIFFIN and B. RADHAKRISHNAN are with Department of Materials Science and Engineering, University of Alabama at Birmingham, Birmingham, Ala.

Introduction

The microstructure of the fusion zone (FZ) in α_2 titanium aluminide is known to depend upon the weld cooling rate (Refs. 1–3). The as-welded microstructure in the FZ ranges from a retained ß microstructure in the case of a laser weld (Refs. 3, 4) to a series of nonequilibrium microstructures of varying morphology at lower cooling rates as the ß phase transforms to a fine acicular α_2 phase (Refs. 1–3). The FZ hardness in the as-welded condition is the lowest for the retained ordered ß microstructure (Ref. 4) and increases whenever ß transforms to the fine, acicular α_2 phase (Ref. 2).

A study on a Ti-27.8Al-11.7Nb (at.-%) alloy by Strychor, *et al.* (Ref. 5), showed that the ß decomposition to α_2 can be suppressed and thus produce a B2 (CsCl) type structure if rapidly cooled from above the ß solvus. This study also showed the formation of an "ω-type" phase subsequent to B2 ordering. This microstructure has a "tweed-like" appearance. The formation of the ω-type phase occurs during rapid cooling from the disordered ß phase. The tweed microstructure can only be seen using transmission electron microscopy (TEM) with (110) imaging. Based on the premises made in the Strychor, *et al.* (Ref. 5), study, Baeslack, *et al.* (Ref. 4), utilized a pulsed Nd:YAG laser to generate a rapidly cooled fusion zone microstructure in Ti-14Al-21Nb comprised of a potentially ductile ordered ß phase. He succeeded in obtaining an average fusion zone hardness that was well below that previously observed in arc welds but greater than the unaffected base metal hardness. The <110> bright-field image did not show the "tweed-like" microstructure indicative of complete retention and ordering of the ß phase.

PWHT has been shown to reduce or remove residual stress and to improve fracture toughness as a result of stress relief in most metals (Ref. 6). Thus, it is expected that better control of the FZ mechanical properties of Ti-14Al-21Nb can be obtained through PWHT. However, there is relatively little published work on the effect of postweld heat treatment on the fusion zone microstructure of α_2 tita-

KEY WORDS

Heat Treatment
Ti-14Al-21Nb Alloy
GTA Spot Welds
PWHT
Fusion Zone Hardness
Fusion Zone Struct.
Weld Microstructure
Weld Cooling
Stress Relief
Microhardness

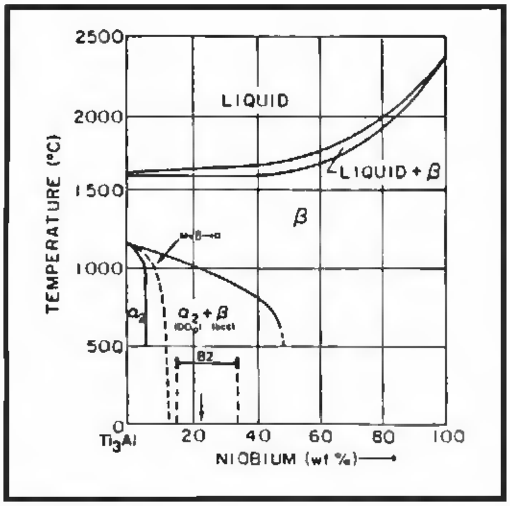

Fig. 1 — Pseudo-binary phase diagram for Ti_3Al-Nb (Ref. 5).

nium aluminide. An investigation of PWHT of α_2 titanium aluminides was done by Baeslack, *et al.* (Ref. 7). He took pulsed, laser-welded samples and subjected them to 4 h heat treatments at 650°, 750° and 850°C (1202°, 1382° and 1562°F). It was concluded that the bend ductility of the pulsed, laser beam welded samples increased with increasing PWHT temperature. Significant variations in hardness and microstructure within the fusion zone were attributed to macroscopic compositional fluctuations associated with pulsed laser beam welding.

This research investigated the effect of different postweld heat treatments on the fusion zone structure and hardness of an α_2 titanium aluminide that was spot welded with gas tungsten arc (GTA) welding. The purpose of this paper is to characterize the GTAW FZ microstructure of Ti-14Al-21Nb (wt-%) in the as-welded and PWHT conditions and to relate the microstructures to the hardness.

Procedure

Gas tungsten arc spot welds were made on 1 x 0.5 x 0.018-in. (2.54 x 1.27x 0.0457-cm) samples of Ti-14Al-21Nb. The composition of the alloy used in this study is denoted approximately by the arrow on the Ti_3Al-Nb pseudo-binary phase diagram in Fig. 1. Samples were welded using a configuration which yielded a rapid weld cooling rate and reduced atmospheric contamination. The samples were placed on a copper block to facilitate fast cooling and spot welded while enclosed in a Lucite® box containing argon to reduce atmospheric contamination. The welding configuration consisted of the torch being clamped to a stand in order to insure for all samples that the distance from the torch to the sample was the same. All samples were welded for 3 s at 32 A and 17 V. This produced a full penetration molten weld pool that was 6-mm (0.24 in.) diameter on top.

The fusion zones were carefully cut with the use of a low-speed diamond saw. After cleaning in an acetone ultrasonic bath, some of the samples were sealed in quartz tubes, which were evacuated and backfilled with argon. The remainder of the samples were either left in the as-welded condition or placed into stainless steel bags for heat treating.

Postweld heat treatments were performed at two temperatures: 650°C (1202°F) and 980°C (1796°F). The purpose of choosing the 650°C PWHT was to transform the as-welded microstructures above the ω-solvus temperature. The ω-solvus temperature for Ti-14Al-21Nb is not available in the literature. However, an estimate of 450°C (842°F) was made, based on data from Collings (Ref. 8) for other α/ß titanium alloys. The 980°C temperature was chosen to give faster transformation kinetics in the same phase field. Samples, sealed in quartz tubes, were exposed to 1-, 4-, 12- and 50-h postweld heat treatments at 650°C. A second set of samples was PWHTed for 0.5-, 1-, 2- and 4-h at 980°C. These heat treatments were done in a box furnace. The samples were quenched in water after heat treatment. The 1-min heat treatments at 650° and 980°C were performed with samples placed inside stainless steel bags. Temperatures were accurately measured by placing a Type K thermocouple in contact with the sample inside the stainless steel bag. The heat treatment bag was slid into a tube furnace with a push rod. During heat treatment at 650°C, the specimen spent 136 s between 450° and 650°C and an additional 60 s at 650°C. During the 980°C PWHT, the time elapsed between 450° and 980°C was 42 s, with an additional 60 s at 980°C. The samples were water quenched immediately following heat treatment.

Metallographic preparation consisted of grinding with 320- through 600-grit silicon carbide, rough polishing with 6- and 3-micron diamond paste, followed by final polishing with 0.06-micron colloidal silica. The samples were then etched with Kroll's reagent (2mL HF, 5mL HNO_3, and 100 mL H_2O). Vickers microhardness data were obtained from these samples with a load of 1000 g.

The fusion zones were prepared for transmission electron microscopy (TEM) evaluation as follows. The samples were first ground to a thickness of 100 µm. A 3-mm disk was cut from the centers of each fusion zone with a metal punch. Thinning of the disks was done on a jet polisher with an electrolyte which consisted of 300 mL methanol, 30 mL perchloric acid, and 175 mL butanol. The thinning conditions were –40°C (–40°F) and 15 V for the as-received and as-

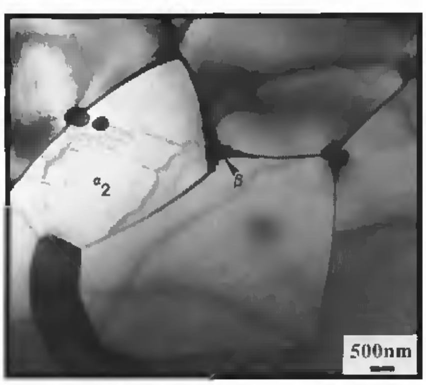

Fig. 2 — TEM bright-field micrograph of as-received Ti-14Al-21Nb.

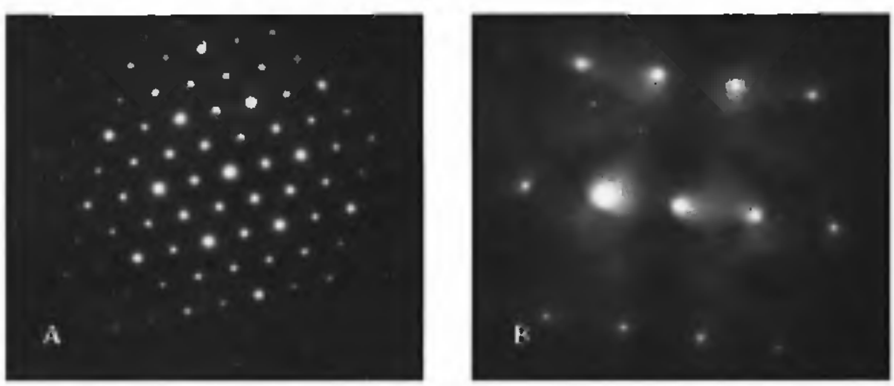

Fig. 3 — Selected area diffraction (SAD) patterns. A — α_2 matrix; B — ß precipitate from as-received Ti-14Al-21Nb.

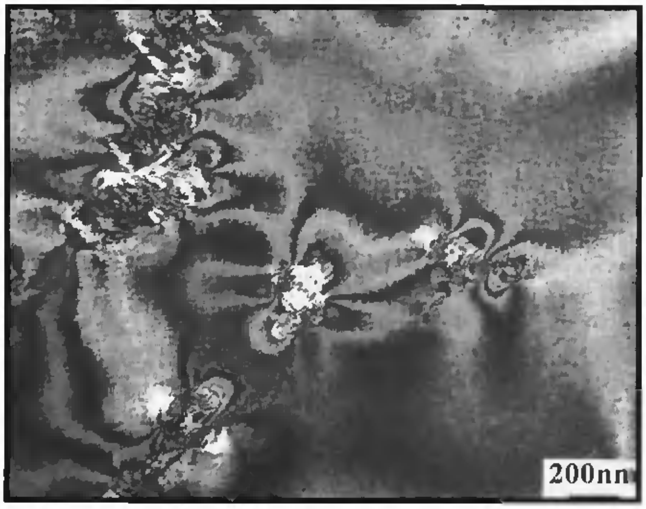

Fig. 4 — TEM <110> bright-field image of the as-welded condition.

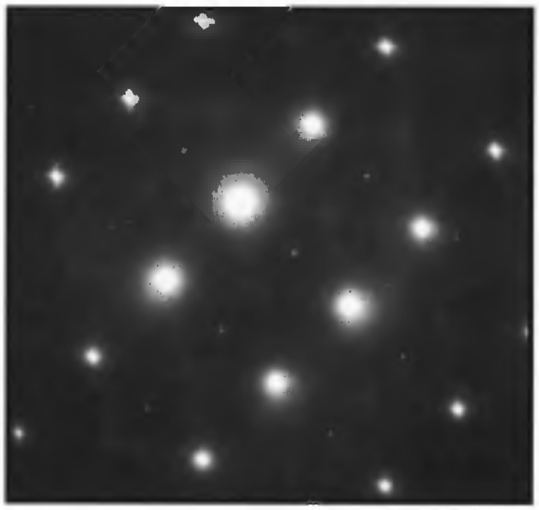

Fig. 5 — Representative [$\bar{1}10$]β SAD pattern from the as-welded condition.

welded samples and –40°C and 45 V for all heat treated samples. TEM evaluation was performed using a JEOL 2000FX microscope.

Results

As-Received Condition

The as-received material was checked to verify that it consisted of equiaxed α_2 grains with ß at grain boundaries as stated in various references (Refs. 1–4). Figure 2 shows a TEM micrograph of this condition where the matrix proved to be α_2 and the precipitates β. This was confirmed with selected area diffraction (SAD) patterns that were taken from the matrix (Fig. 3A) and precipitates (Fig. 3B).

As-Welded Condition

Samples in the as-welded condition were investigated using optical and TEM techniques. Observation under an optical microscope showed that the fusion zone appeared to be featureless. The TEM ($\bar{1}10$) bright-field image of the as-welded sample is shown in Fig. 4. It is quite evident from Fig. 4 that the fusion zone is not featureless, but consists of a "tweed-like" microstructure. Figure 5 shows a [$\bar{1}10$]ß zone SAD pattern that was taken from this area. The appearance of streaking in the diffraction pattern is characteristic of the tweed-like microstructure obtained by rapid cooling rates as was shown by Strychor, *et al.* (Ref. 5). The tweed microstructure was found in all as-welded samples in this study. As expected, the SAD patterns showed that the microstructure consisted of B2 (ordered ß) + ω with no evidence of α_2 being present.

Microhardness Profiles

The microhardness data were plotted as Vickers hardness number (VHN) vs. distance from the weld centerline for the as-welded and each PWHT condition. Figure 6 shows the hardness profiles for the as-welded and the 650°C PWHT conditions. An important feature of the 650°C PWHT was the hardness values were higher than those in the as-welded condition. This hardening persisted during PWHT at 650°C for about 4 h. A significant reduction in hardness occurred between 4 and 12 h. The average fusion zone hardness values for 12 and 50 h at 650°C were near that of the base metal.

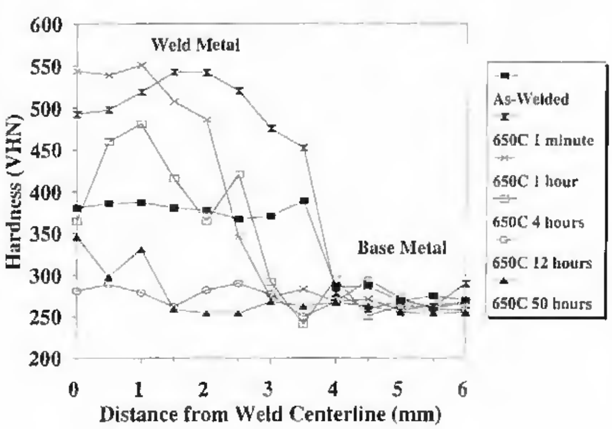

Fig. 6 — Microhardness profiles for the 650°C PWHT.

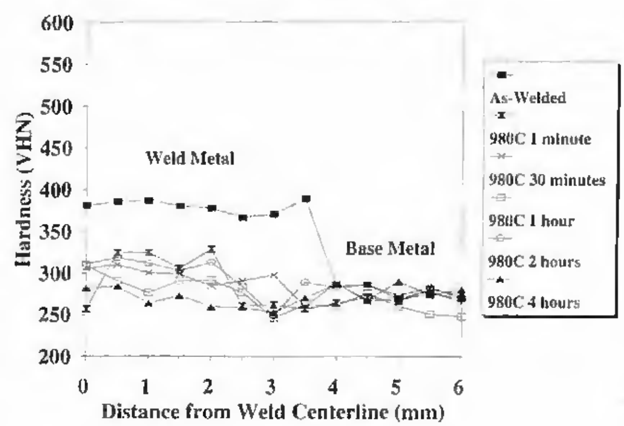

Fig. 7 — Microhardness profiles for the 980°C PWHT.

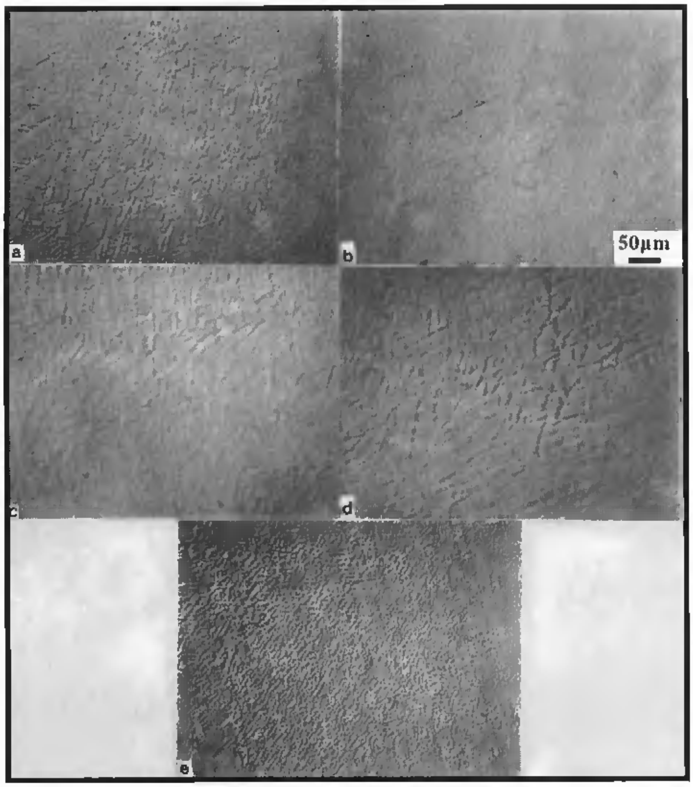

Fig. 8 — Light micrographs for the 650°C PWHT.

The microhardness profiles obtained for each PWHT at 980°C are shown in Fig. 7. The average fusion zone hardness for 1 min at 980°C was lower than that of the as-welded condition but was higher than the base metal hardness. The profiles for the 0.5-, 1-, 2- and 4-h PWHTs were all very similar. The fusion zone hardness decreased with increasing time. The average fusion zone hardness for each was near that of the base metal.

Microstructures for 650°C PWHT

The light micrographs from the fusion zones of each PWHT at 650°C appear to be featureless (Fig. 8). A TEM study showed that at higher magnification many microstructural features were resolvable.

The dominant microstructure after 1 min at 650°C is shown in Fig. 9A. This area shows the early formation of α_2-laths. A representative SAD pattern from this area (Fig. 9B) contains superlattice reflections which are characteristic of ordering. All of the SAD patterns collected for the 650°C, 1 min PWHT showed that α_2 was the only phase present for this thermal cycle.

After 1 h at 650°C, the microstructure consisted of well-defined α_2-laths. This is shown in Fig. 10A. The convergent beam diffraction (CBD) pattern from this area (Fig. 10B) shows that this structure is ordered. At this PWHT, CBD and SAD patterns showed that α_2 was the only phase present.

The 650°C, 4-h PWHT contained two distinct microstructures. The SAD patterns from these areas had no symmetry and the identity of the structures could not be determined. The microstructures consisted of lath regions (Fig. 11A) and needle-like regions (Fig. 11B). The needle-like regions appeared to be the more dominant microstructure at this PWHT. The only phase identifiable from diffraction patterns was α_2.

Twelve hours at 650°C also yielded two distinct microstructures. Some areas had a few laths present along with some relatively large clear grains (Fig. 12A). Other areas had a needle-like microstructure present (Fig. 12B). The only phase that could be distinguished at this PWHT was ordered α_2.

The 650°C, 50-h PWHT had three distinct microstructures present. Figure 13 was taken from a representative area at a low magnification in order to show the relationship between the three different microstructures. The microstructures consisted of areas with laths [1], lath "remnants" [2], and clear grains with a low-dislocation density [3]. The needle-like microstructure was not present after 50 h at 650°C; however, it is believed that it eventually formed the areas located between the laths. Figure 14 was taken from the lath "remnant" region, which was dominant at this heat treatment, at a higher magnification. SAD patterns from the lath remnant areas showed that the lath remnant region is ordered. The only phase that could be identified after 50 h at 650°C was α_2.

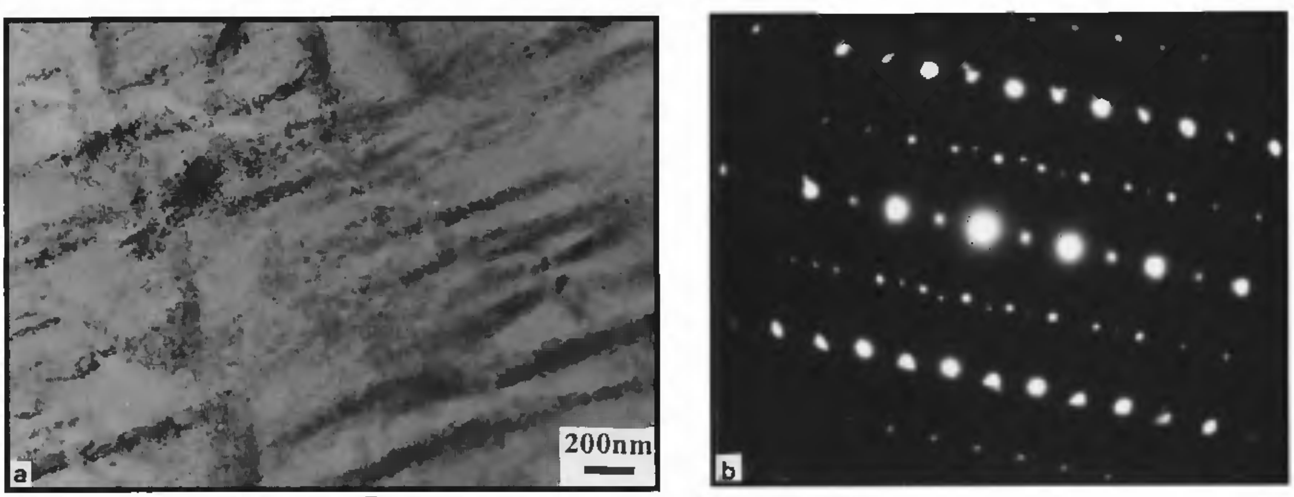

Fig. 9 — A— Bright-field image; B — $[\bar{1}100]$ α_2 SAD pattern from the 650°C, 1 min PWHT.

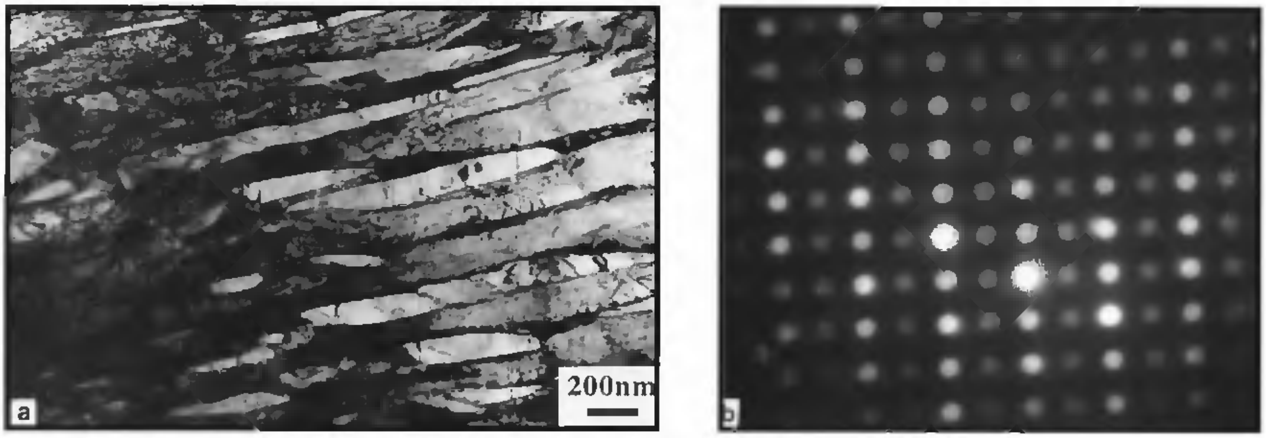

Fig. 10 — A — Bright-field image; B — convergent beam diffraction (CBD) pattern from the 650°C, 1-h PWHT.

Microstructures for 980°C PWHT

The optical micrographs from the fusion zones of PWHTs at 980°C have distinctive features unlike the optical micrographs of the 650°C PWHT fusion zones — Fig. 15. There were two distinct microstructures obtained for the 980°C, 1-min PWHT. A low-magnification micrograph (Fig. 16) shows the relative locations at which the two microstructures appear. There were clear grains present along with high-dislocation density lath regions. The clear grains (denoted by arrows in Fig. 16) were not the dominant regions. These regions were narrow and extended throughout the sample in a zigzag manner. It is believed that these clear α_2 grains occurred at prior-ß grain boundaries. This recrystallization of α_2 grains at prior-ß grain boundaries has also been observed by previous researchers (Refs. 7, 9). The clear grain regions were surrounded by the dominant, fine-grained, lath regions. The SAD patterns showed that both regions were ordered. The only phase that could be identified at this PWHT was α_2.

The remaining PWHTs at 980°C (0.5, 1, 2 and 4 h) all had the same two distinct microstructures. One microstructure consisted of subgrains of α_2 with a high dislocation density and intragranular B2 precipitates. The other consisted of clear α_2 grains with intergranular B2. The presence of the metastable B2 structure is believed to be due to the fact that the samples were water quenched after heat treating. Representative micrographs for the 0.5-, 1-, 2- and 4-h thermal cycles at 980°C are shown in Fig. 17. Figure 17A shows the α_2 subgrains with intragranular B2, and Fig. 17B shows the clear α_2 grains with intergranular B2. All of these PWHTs had the same phases present: α_2 and B2. Figure 18 shows a region from the 2-h PWHT sample where the clear α_2 grains were located directly adjacent to α_2 subgrains that contained dislocations and B2. The SAD patterns verified that the phases at the 980°C PWHT for 0.5-, 1-, 2- and 4-h were α_2 and B2.

Lath Size

Quantitative microscopy involved the measurement of lath size in samples subjected to 650°C PWHT. The point count method was used to determine the volume fraction (V_v) and the line-intercept count method was used to determine the surface area per unit volume (S_v). Both V_v and S_v were used to determine the average lath size (λ_L). The data obtained were used to discuss the variation of microhardness with microstructural changes during the 650°C PWHT. The lath size or spacing was not found for the 1-min and 12-h PWHTs at 650°C because it was difficult to distinguish the laths from the surrounding features in these two cases.

Discussion

The as-received material used in this study consisted of equiaxed α_2 grains with ß at grain boundaries. A tweed-like microstructure of transformed ß (Ref. 4) was obtained in the fusion zone after welding. This ω-type phase formed from the B2 structure as a result of rapid cooling from the disordered ß phase.

This structure produced a VHN that was approximately 100 VHN higher than the as-received condition. There was no α_2 phase found in the as-welded condition.

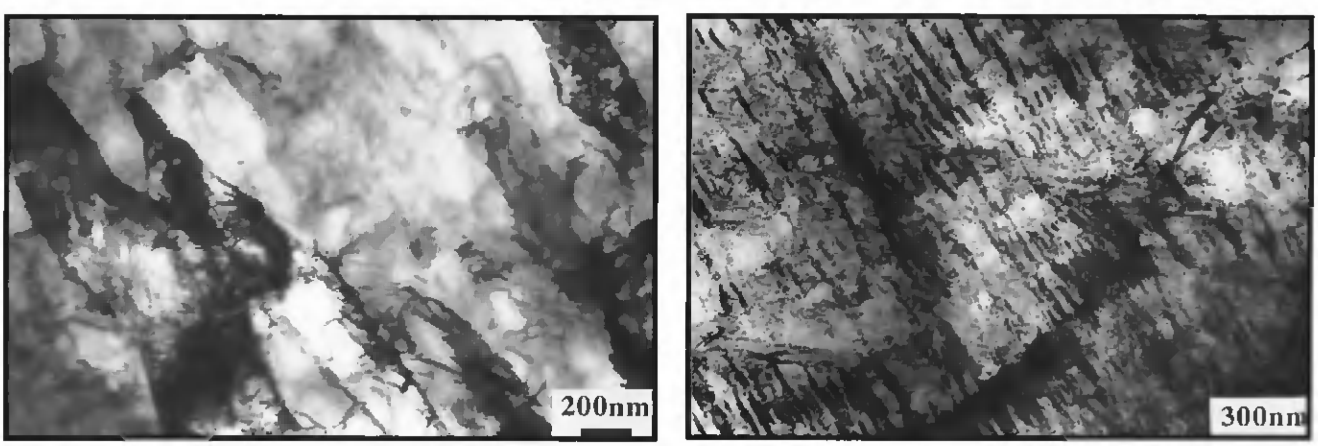

Fig. 11 — Bright-field images showing the microstructures obtained for 650°C, 4 h. A — laths; B — needle-like structure.

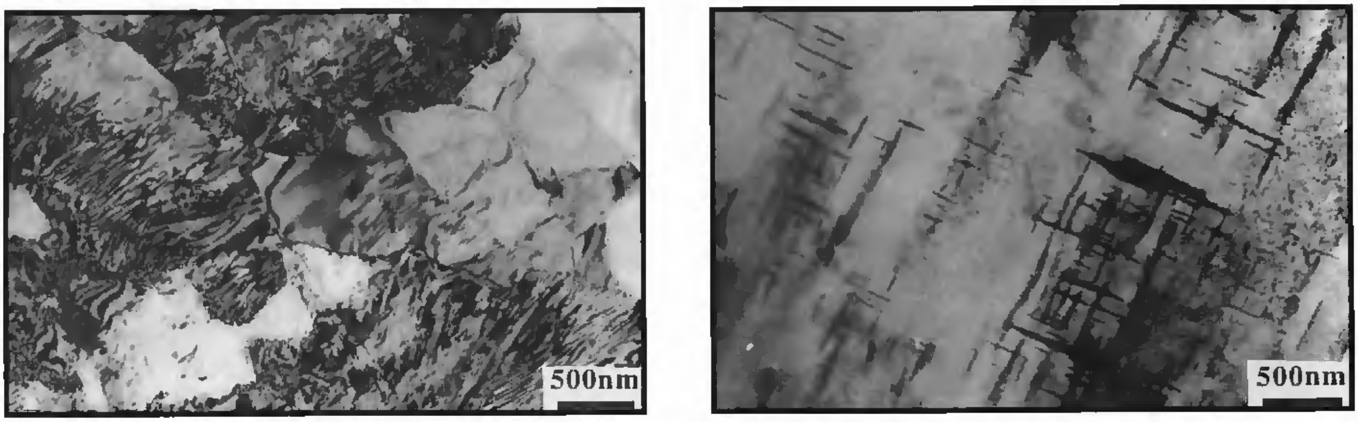

Fig. 12 — Bright-field images from the 650°C, 12-h PWHT. A — clear grains with laths region; B — needle-like region.

Fig. 13 — Bright-field image of the three distinct microstructures present after 50 h at 650°C: [1] laths; [2] lath "remnants"; and [3] clear grains.

Microstructure Evolution at 650°C

The path of microstructural evolution as a function of increasing time at 650°C consisted of the early formation of laths at one minute (Fig. 9A) that became well defined laths after 1 h — Fig. 10A. After 4 h (Fig. 11), the microstructure consisted of both lath regions and needle-like regions, which were the dominant structure. The microstructure then changed to a structure that contained laths, clear grains and a few needle-like regions after 12 h — Fig. 12. As stated earlier, only a visual description of the lath and needle-like microstructures was given because SAD patterns from these regions were very distorted and had no symmetry. Therefore, the authors were unable to identify the structures. The microstructural evolution at 650°C was examined for up to 50 h. The microstructure for the 650°C, 50-h thermal cycle consisted of laths, lath "remnants," and clear grains at prior-β grain boundaries — Fig. 13.

The scatter in data for 4 h compared to the scatter in data for all the other times at 650°C suggest that the microstructure is in transition at this time. The microstructures that were obtained at 4 h support this assumption. The dominant microstructure for all times except 4 h was some type of lath microstructure. At 4 h, the lath microstructure was present but the predominant microstructure was needle-like. The transition from a lath to a needle-like morphology is believed to be responsible for the large scatter in hardness data that occurred at 4 h and 650°C.

The ω-type tweed microstructure was not present in any of the PWHTs at 650°C. The laths that were present in the majority of the microstructures for the 650°C PWHTs grew with increasing time at 650°C. This is shown in Fig. 19, which is a plot of lath size vs. time. The microstructure observed for the 650°C, 1-min thermal cycle was referred to as "early formation of laths" because of the appearance of the laths. The edges of the laths were not very sharp or well defined like the laths that were present for the 650°C, 1-h thermal cycle. There was also a microstructure obtained at 650°C, 1 min that had a mottled appearance similar to that of the tweed structure that was obtained for the as-welded condition. However, unlike the tweed structure, the SAD patterns for this structure showed that there was no streaking and that α_2

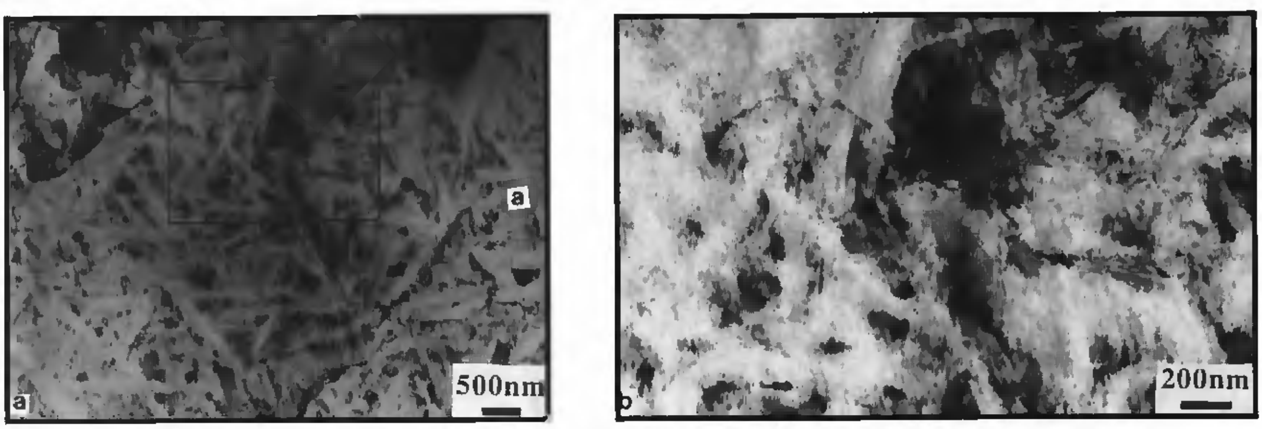

Fig. 14 — High-magnification bright-field image of region [2] (lath "remnants") in Fig. 13.

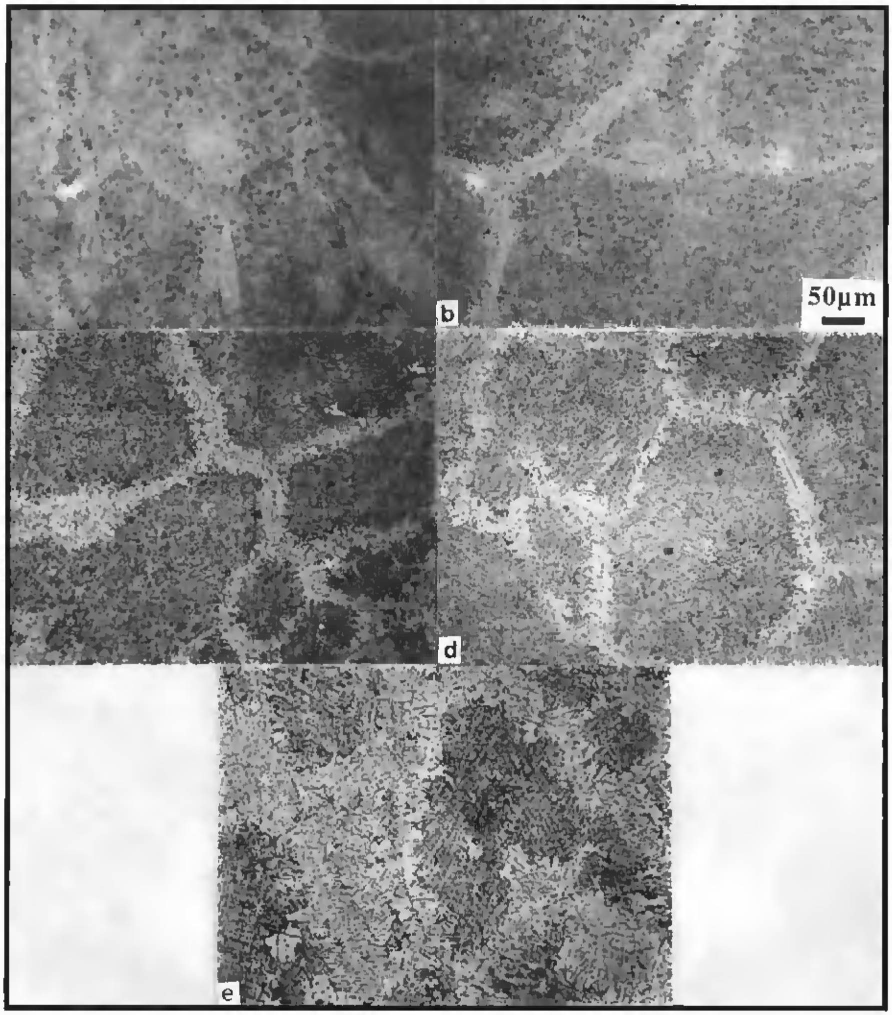

Fig. 15 — Light micrographs for 980°C PWHT.

was the only phase present. It was found that the lath microstructure reached its peak dominant presence at 1 h.

The progression of the lath microstructure evolution with time at 650°C eventually led to the formation of clear α_2 grains. It was not evident from light micrographs, but TEM micrographs showed that the clear α_2 grains formed at prior-ß grain boundaries. This was consistent with the results of PWHT work by Baeslack, *et al.* (Ref. 7). It is also believed that the needle-like phase became the areas that separated the laths from one another. These conclusions are supported by the fact that the laths grew and reoriented to the point where it was hard to distinguish them within the grains. This is confirmed by the SAD pattern in Fig. 20, which shows that the laths appear to be approaching a single orientation after 50 h at 650°C. Only α_2 was found in the lath and lath "remnants" regions. These conclusions are also supported by the fact that a lath microstructure that consisted of only α_2 was observed after 1 min at 980°C, but not for the other PWHT at 980°C where the α_2 + B2 microstructure was present. The laths that were present after 1 min at 980°C had microhardness and lath size values that were similar to those of the 650°C 50-h thermal cycle. This suggests that the lath microstructures that formed for the 650°C PWHT were present for very short times at 980°C. Since no laths were present for the 0.5-, 1-, 2- and 4-h PWHT, it is believed that the laths observed at 980°C, 1 min eventually formed the clear α_2 grains present at other times.

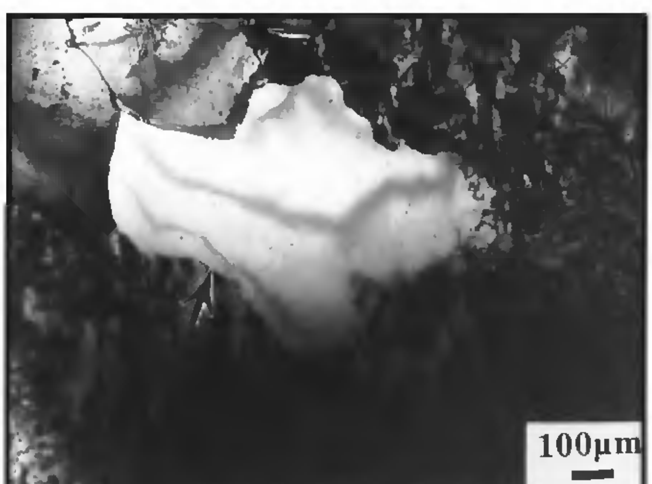

Fig. 16 — Bright-field image of 980°C, 1-min PWHT. Arrows denote the clear α_2 grains at prior-ß grain boundaries.

Microstructure Evolution at 980°C

There were two distinct α_2 + B2 microstructures that occurred for all of the 980°C PWHT except for the 1-min thermal cycle. One consisted of α_2 subgrains (recovering laths) with intragranular B2 precipitates and dislocations while the other had clear α_2 grains with intergranular B2. It is believed that the clear α_2 grains + B2 microstructure formed after the completion of the lath progression sequence. This conclusion is supported by the 650°C PWHT lath progression sequence and by the microstructure of 980°C, 1-min thermal cylce. Observation of the lath progression sequence for the 650°C thermal cycles suggested that the laths eventually formed clear α_2 grains. The laths that were present in the 980°C, 1-min thermal cycle (Fig. 16) were similar in size to the lath regions (Fig. 13, [1]) that were found in the final 650°C thermal cycle (50 h). The process of the laths forming clear α_2 grains is similar to the recovery of martensite in steel (Ref. 10). The progression of laths to clear α_2 grains and the fact that laths present at the 980°C, 1-min thermal cycle had similar characteristics to the laths present at the 650°C, 50-h PWHT suggests that the path that led to the formation of the α_2 + B2 microstructure was as follows: ω-type (tweed) $\rightarrow \alpha_2$ (laths) $\rightarrow \alpha_2$ + ß $\rightarrow \alpha_2$ + B2.

It was noticed that all of the thermal cycles at 980°C except the 1-min thermal cycle had microhardness profiles that were very similar (Fig. 7). It was also shown in Figs. 17 and 18 that the microstructures for these thermal cycles were similar and consisted of different morphologies of α_2 + B2. Therefore, it was observed that the microhardness profiles for these PWHTs were similar because their corresponding microstruc-

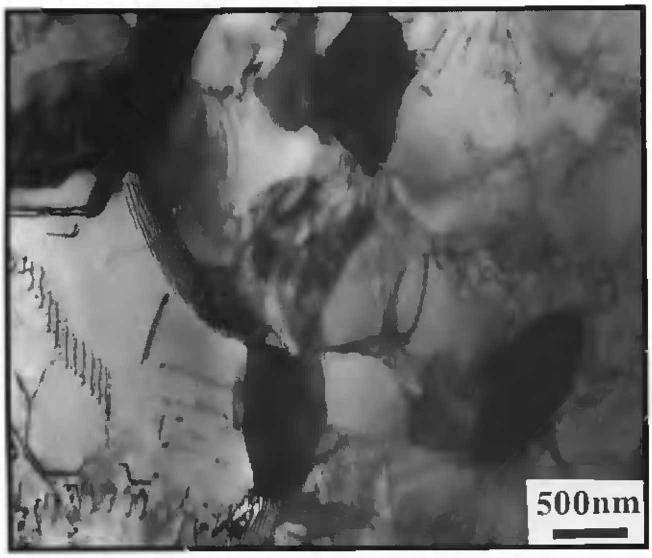

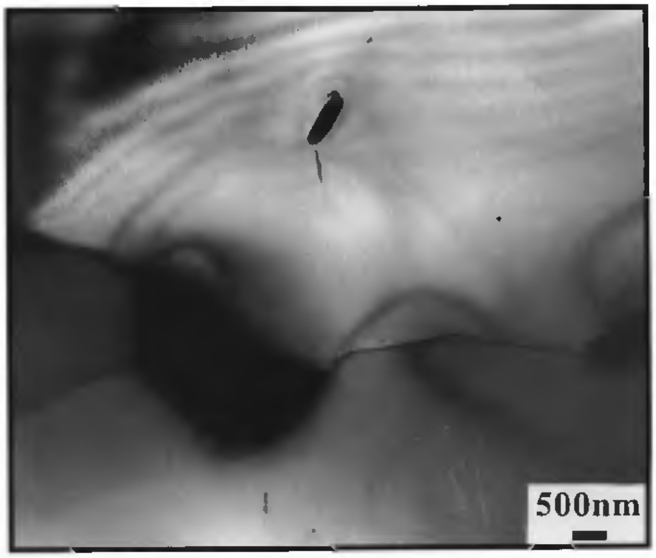

Fig. 17 — Bright-field images of the microstructures present for the 0.5-, 1-h, 2-h and 4-h thermal cycles at 980°C. A — α_2 subgrains + intragranular B2; B — clear α_2 grains + intergranular B2.

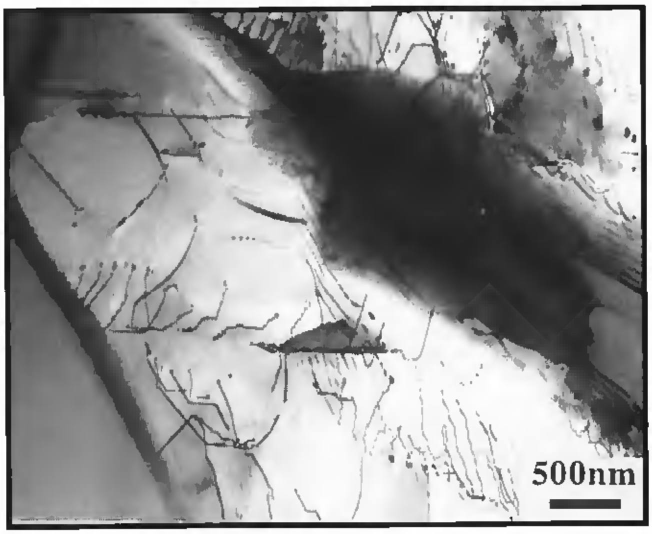

Fig. 18 — Bright-field image which shows clear α_2 grains directly adjacent to α_2 subgrains that contain dislocations.

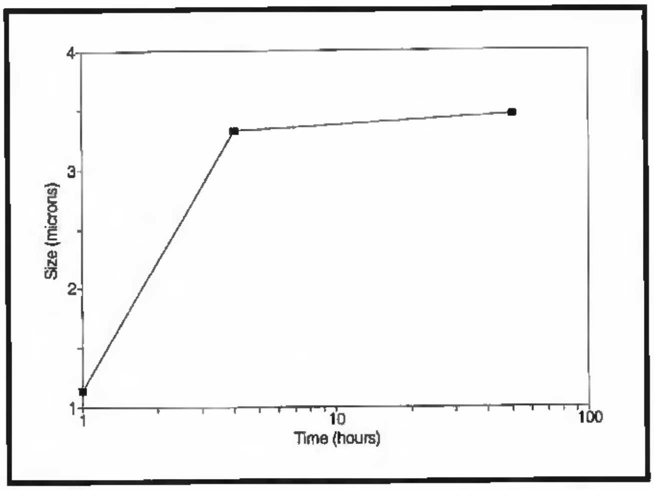

Fig. 19 — Lath size vs. time for the 650°C thermal cycles.

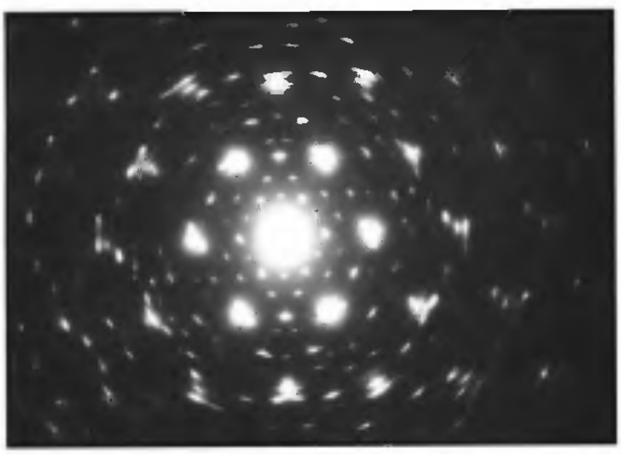

Fig. 20 — SAD pattern of lath region shown in Fig. 13. This SAD pattern shows that the laths appeared to be approaching a single orientation after 50 h at 650°C.

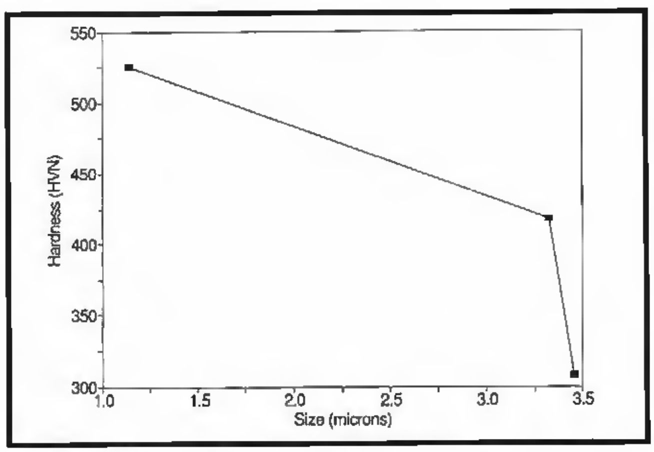

Fig. 21 — Fusion zone hardness vs. lath size for the 650°C thermal cycles.

tures were very similar. The hardness values of the 980°C, 1-min thermal, and the 650°C, 50-h thermal cycles were the same statistically. The average hardness for the 650°C, 50-h, and 980°C, 1-min thermal cycles were 309 VHN (standard deviation = 38.6) and 290 VHN (standard deviation = 34), respectively.

This study also showed that there was a noted relationship between the microhardness and lath size. The hardness profiles in Fig. 5 showed that the fusion zone microhardness decreased as the time increased. It was observed that a direct relationship between microhardness in the fusion zone and time can be made. It is also shown in Fig. 19, which is a plot of lath size vs. time, that the lath size increased as the time of PWHT at 650°C increased. Thus, from these facts, a plot of fusion zone hardness vs. lath size can be constructed. This plot is shown in Fig. 21, which shows that one relationship observed between microhardness and microstructure at 650°C was that the microhardness decreased as a function of increasing lath size.

Conclusions

This study set out to investigate the effect that postweld heat treatment thermal cycles had on the fusion zone properties of an α_2 titanium aluminide, Ti-14Al-21Nb. The as-welded ω-type phase microstructure had a tweed-like, mottled appearance, which produced a microhardness that was approximately 100 VHN higher than the as-received microhardness. The as-received microstructure consisted of equiaxed α_2 grains with ß at grain boundaries.

Postweld heat treatment at 650°C eliminated the ω-type phase, but the initial α_2 lath structures that formed caused secondary hardening above that of the as-welded condition. The fusion zone microhardness eventually decreased to values lower than the as-welded condition when longer thermal cycles (12 and 50 h) were employed at 650°C. One factor found to contribute to the decrease in microhardness was the coarsening of the lath microstructure with increasing time at 650°C.

Postweld heat treatment at 980°C resulted in two distinct α_2 + B2 microstructures. One consisted of high-dislocation density α_2 subgrains with intragranular B2 precipitates, the other consisted of clear α_2 grains with intergranular B2. This PWHT reduced the hardness to values near that of the as-received condition at a much faster rate than the 650°C PWHT. Microstructure evolution was found to follow the sequence: ω-type (tweed) $\rightarrow \alpha_2$ (laths) $\rightarrow \alpha_2$ + ß $\rightarrow \alpha_2$ + B2.

References

1. David, S. A., Horton, J. A., Goodwin, G. M., Phillips, D. H., and Reed, R. W. 1990. Weldability and microstructure of a titanium aluminide. *Welding Journal* 69(4): 133-s to 140-s.

2. Baeslack, W. A., Mascorella,T. J., and Kelly, T. J. 1989. Weldability of a titanium aluminide. *Welding Journal* 68 (12): 483-s to 498-s.

3. Cieslack, M. J., Headley, T. J., and Baeslack, W. A. 1990. Effect of thermal processing on the microstructure of Ti-26A1-11Nb: Applications to fusion welding. *Met. Trans. A.*, 21A: 1273 to 1286.

4. Baeslack, W. A., Cieslak, M. J., and Headley, T. J. 1988. Structure, properties and fracture of pulsed Nd:YAG laser welded Ti-14.8wt%Al-21.3wt%Nb titanium aluminide. *Scrinta Met.* 22(7): 1155 to 1160.

5. Strychor, R., Williams, J. C., and Soffa, W. A. 1988. Phase transformations and modulated microstructures in Ti-Al-Nb alloys. *Met. Trans. A.*, 19A: 225 to 234.

6. Lancaster, J. F. 1987. *Metallurgy of Welding.* Allen & Unwin, London, England, pp. 91–93.

7. Baeslack, W. A., Cieslak, M. J., and Headley, T. J. 1990. Heat treatment of pulsed Nd:YAG laser welds in a Ti-14.8wt%Al-21.3wt%Nb titanium aluminide. *Proceedings of the Second International Conference on Trends in Welding Research.* eds. S. A. David and J. M. Vitek, ASM International, Materials Park, Ohio, pp. 211–216.

8. Collings, E. W. 1984. *The Physical Metallurgy of Titanium Alloys.* ASM International, Materials Park, Ohio, pp. 76–82.

9. Mascorella, T. J. 1987. Weldability of a Ti_3Al-Nb alloy. Master's thesis, The Ohio State University, Columbus, Ohio.

10. Griffin, R. D. 1989. The effects of heat treatment and radiation on a low activation martensitic stainless steel. Ph.D. dissertation, The University of Wisconsin-Madison, Madison, Wis.

RESEARCH/DEVELOPMENT/RESEARCH/DEVELOPMENT/RESEARCH/DEVELOPMENT/RESEARCH/DEVELOPMENT